communications biology

A Nature Portfolio journal

Article

https://doi.org/10.1038/s42003-025-08758-6

An effective system for senescence modulating drug development using quantitative high-content analysis and high-throughput screening

Yajie Hu, Xueqi Xue, Tian Han, Ye Li, Tonghui Zhang, Tao Lu & Peichuan Zhang

Study of cellular senescence is critical in aging research and anti-senescence therapy drug development. Current methods for the evaluation of the widely accepted cellular senescence marker senescence-associated beta galactosidase (SA-β-gal) activity assay rely on bright-field imaging, which is non-quantitative and tedious to perform. We have developed an effective and reproducible multiplex high-content analysis system for high-throughput screen and evaluation of senescence modulators. The IC_{50} or EC_{50} of the senescence modulators on fibroblasts were determined, which are essential for drug development and have not been able done before. In a single high-throughput screen, all three types of senomorphic, senolytic, and seno-inducing agents can be evaluated effectively. Using our system, we have identified new molecular entities that modulate MMC-induced senescence in fibroblasts through potential new cellular targets.

Cellular senescence plays important roles in development and aging, as well as in many types of diseases[1]. Modulation of senescence has been implicated in therapeutic strategies against aging, cancer, autoimmune and other diseases[2,3]. Traditionally, senescent cells are identified with senescence-associated β-galactosidase (SA-β-gal) activity (pH 6.0) measurement of the colorimetric signals of its staining substrate 5-bromo-4-chloro-3-indolyl β-D-galactopyraniside (X-gal)[4], or p53 and $p16^{INK4a}$ expression[5–7] among the markers[8]. In majority of the described methods, bright-field imaging was used to capture X-gal precipitate signal for manual or automated analysis[9]. Several methods have been described recently for detecting β-galactosidase activity in senescent cells and cancer cells with newly developed fluorescent dyes like 5-dodecanoylaminofluorescein di-β-D-galactopyranoside (C_{12}FDG)[10], CellEvent™ Senescence dye, and several selective and activatable fluorescent dyes, e.g., notably KSL11[11] and SPiDER-βGal[12]. Fluorescence substrate C_{12}FDG was also used to measure SA-β-galactosidase activity in live cells via flow cytometry analysis[10]. Label-free cellular morphology analysis with complicated AI algorithm provide an applicable method for high-throughput screening of anti-senescence compounds[13–16]. All of those methods are capable of identifying anti-senescence regents, but with their limitations. None of the forementioned methods offer a complete system for senotherapeutic drug development.

In searching for an effective and reproducible method to screen and evaluate cellular senescence modulators, we adopted the gold-standard for primary cellular senescence detection of X-gal digestion product 5-bromo-4-chloro-3-indolyl (BCI) precipitate but in fluorescence mode. The much neglected fluorescent property of BCI was first reported by Dr. Fritzsch's laboratory[17] and later applied to fluorescent confocal analysis of LacZ reporter in tissue sections by Dr. Cilladiego's team[18]. The use of fluorescence detection of the blue precipitate produced by cleavage of X-gal by SA-β-gal had not been reported for routine experiments and senotherapeutic drug development. The fluorescence method allows the quantification of SA-β-gal activity and automated multiplex imaging for concomitant analysis of multiple factors.

Results and discussion

To study cellular senescence modulators, we first optimized a system that is reproducible in inducing senescent cells. Among the many inducers of cellular senescence, disturbance of genomic integrity is the most common cause[19]. Optimized Mitomycin C (MMC) treatment was chosen for senescence induction in our system for the convenience and reproducibility after several DNA damaging agents including radiation, hydrogen peroxide, and bleomycin, etc. were tested (results not shown)[20]. Cells post senescence induction were fixed with formaldehyde and stained for SA-β-gal activity with X-gal, cytoplasm with F-actin antibody and nuclei with DAPI. Bright-field and fluorescent images were captured using proper excitation and emission wavelengths. Specifically, excitation wavelength of 640 nm and emission wavelength 665-705 nm were used for fluorescence detection of SA-β-gal digestion product according to the previous publications[17,18] Both

Discovery Biology Unit, WuXi Biology, WuXi AppTec Ltd., Shanghai, China. e-mail: tlu101@gmail.com; zhang_peichuan@wuxiapptec.com

bright-field and fluorescence images showed clear signals of SA-β-gal staining that overlaid spatially (Fig. 1a, b). We consistently achieved about 60% of senescent cells after MMC treatment (Fig. 1a, c) with human lung fibroblast WI-38 cells under our experimental condition. The fraction of SA-β-gal positive cells from automatic counting in fluorescence images is in agreement with that from manual counting in bright-field images (Fig. 1c and Supplementary Table 1).

To validate our MMC-induced senescence and fluorescence analysis system, we tested different fibroblast cell lines and high-content systems (HCS), as well as other characteristics of cellular senescence. Similar degrees of senescence induction were achieved with primary human dermal fibroblast HDFα and normal human lung fibroblast IMR-90 cells (Supplementary Fig. 1a, c, e), which was confirmed by the higher fraction of cells with enlarged cell and nuclear sizes (Supplementary Fig. 1b, d, f; Supplementary Fig. 2b, d), carried out by automated fluorescent high-content analysis. The feasibility and reproducibility of the image acquisition and analysis were tested on two HCS systems (CQ1 and Operetta) with either laser or LED light sources (Supplementary Fig. 2a–d). The reduced numbers of SA-β-gal positive cells after treatment with Rapamycin, a known senescence inhibitor[21], with our own verification of several senescence markers, including senescence-associated secretory phenotype (SASP) cytokines (IL-6, CXCL1, and HGF)[8,22] and cyclin-dependent kinase inhibitors ($p16^{INK4a}$ and $p21^{CIP1/WAF1}$) (Supplementary Fig. 3a–d)[8,23], further proved the effectiveness of our MMC-induced senescence system and the fluorescence image capture and analysis system.

In drug development, the determination of the IC_{50} or EC_{50} of a compound is crucial for the evaluation of the drug potency and for the structure-activity relationship (SAR) study. Up-to-now, there is no documented method for direct evaluation a compound's potency on modulating cellular senescence. We wondered if the IC_{50} or EC_{50} of a senescence modulator could be determined using our method, since we have demonstrated our method capable of reliable reproducibility in senescence induction with different fibroblast cell lines, in capturing SA-β-gal fluorescence signal, and in automated counting SA-β-gal positive cells in fluorescence images. We plotted fraction of SA-β-gal positive cells treated under different rapamycin concentrations and obtained, for the first time, the IC_{50} at 1.367 nM of rapamycin inhibiting MMC-induced WI-38 cell senescence, and the results were reproducible (Fig. 1d–f). Reported result of rapamycin in the treatment of senescent hCPCs is consistent with our titration with measurable anti-senescence effects starting at about 1 nM and reaching maximal efficacy at approximately 100 nM[24]. Using the same method, we determined the IC_{50}s of two other well-known senescence modulators, senomorphic KU-60019[25] and senolytic Dasatinib and Quercetin[26] (Supplementary Figs. 4a, b, and 5a, b). We also used another senescence marker $p16^{INK4a}$ for the evaluation of rapamycin potency inhibiting fibroblast senescence and obtained an IC_{50} value of 1.25 nM, similar to that using SA-β-gal as marker (Fig. 1e, f; Supplementary Fig. 6a, b). In summary, these results demonstrate that our method is suitable for determining the IC_{50} or EC_{50} values of pro- and anti-senescence modulators. With proper design of compound titration range, this method would also offer a reliable way for studying the biphasic effects of some senescence modulators like Resveratrol[27].

To further demonstrate the robustness of our system, we carried out a proof-of-concept screening for fibroblast senescence modulators in a library of 2560 small molecule compounds with mostly known properties. WI-38 cells were first treated with MMC to induce cellular senescence followed by compound treatment at two doses (1 and 10 μM) in duplicate. The cells were fixed and stained, and fluorescent images were captured with the representative images shown (see Fig. 2a, b and Material and Methods for details). On each 384-well assay plate, there were negative and positive controls, including 7 DMSO control wells, 14 MMC-treated wells, and 7 MMC and Rapamycin treated wells. The data from those wells were used for quality control and normalization.

We explored several ways to better separate normal and senescent cells, including direct analysis using the fraction of SA-β-gal positive cells (PositiveRate) and nuclear size (NucleusArea). We found PositiveRate gave reasonably good separation while that for NucleusArea was marginal (Supplementary Fig. 7a, b). In addition, we also investigated the cell area. However, senescent cells overlayed each other frequently, causing erroneous measurements of cell areas by the machine software. After several trials, a mathematic model we developed, named SenoScore which combines weighed PositiveRate and NucleusArea features, improved the screening results by better separating the normal and senescent cells (Supplementary Fig. 7c). Our data analysis workflow for the screening was described in details in Fig. 3a and Supplementary Fig. 8.

To identify candidate compounds inducing or inhibiting fibroblast senescence, the PositiveRate or SenoScore of each compound were calculated as shown in Supplementary Fig. 9a and Fig. 2c, respectively. Compounds with either PositiveRate or SenoScore larger than the mean of all compounds plus 2x standard deviation of all cells were clarified as seno-inducers (that induce cells into senescence). Compounds with either PositiveRate or SenoScore smaller than the mean of all compounds minus 2x standard deviation of all cells were clarified as seno-inhibitors (that inhibit senescence by either senomorphic that prevents cells entering senescence, or senolytic that cause senescent cells to die).

For the comparison, among the top 34 candidates identified as seno-inducers by either PositiveRate or SenoScore, SenoScore method showed advantage over PositiveRate by picking up substantially more (9–3) known seno-inducer (Reported Inducer, true positive) over PositiveRate (Supplementary Fig. 9b). For seno-inhibitors, SenoScore method also showed significant advantage over PositiveRate, with 6–0 known inhibitors (Reported Inhibitor, true positive) identified (Supplementary Fig. 9c).

To distinguish senomorphic and senolytic compounds that both will lower the fractions of senescent fibroblasts, we integrated the cell density per imaging area as additional criterion (Fig. 3a). With the same starting cell densities, senolytic compounds will selectively kill senescent cells thus reduce the number of cells while senomorphic compounds will maintain the same cell density mostly (Supplementary Fig. 8c, equation (6)). With these criteria, we separated senolytic agents from the rest of seno-inhibitors by incorporation of cell number from the same screening experiment in data analysis (Supplementary Fig. 8; Fig. 3a). Indeed, using our mathematic model SenoScore, better classification of compounds screened could be achieved, and the final screening results are presented in Fig. 3b. Among these compounds, the anti-senescence activity of the representative positive control, diphenyleneiodonium chloride, and a newly identified compound was confirmed through IC_{50} titration assays (Fig. 3c, d).

We randomly picked a few novel candidates of senomorphic, senolytic, and seno-inducer for further experimental verification with fresh batch of compounds purchased from the corresponding vendors. For the selected novel compounds, one out of two seno-inducer (50%), 2 out of five senolytics (40%), one out of three senomorphics (33%), were confirmed by dose titration and IC_{50}/EC_{50} determination (Supplementary Fig. 10a, b). From this screen, a compound (CPD-X004), known previously for its activity on target-X but neither itself nor its gene target have been reported to play any role in cellular senescence, was identified to function as a senomorphic reagent. Its senomorphic activity was confirmed by IC_{50} titration and other markers $p16^{INK4a}$ and $p21^{CIP1/WAF1}$ by Western blots (Supplementary Fig. 10b, c). This demonstrate that our method is capable of discovering new drug target as well as new chemical entity.

It is interesting that the seno-inducers identified here function on top of the senescence induction of MMC, suggesting potentially different mechanisms inducing senescence and that they could be used as candidate drugs for combination cancer therapy with a chemotherapy drug. Analysis of the seno-inhibitors reported in the literature and not identified in the experiment reveals that most of these modifiers function through different mechanisms other than DNA damage response (Fig. 3b). Recent data from single-cell analysis[28] as well as the new recommendation of detection criteria[8] may be used to develop new assays for the identification of senescent cells. Different standardized induction methods of cellular senescence

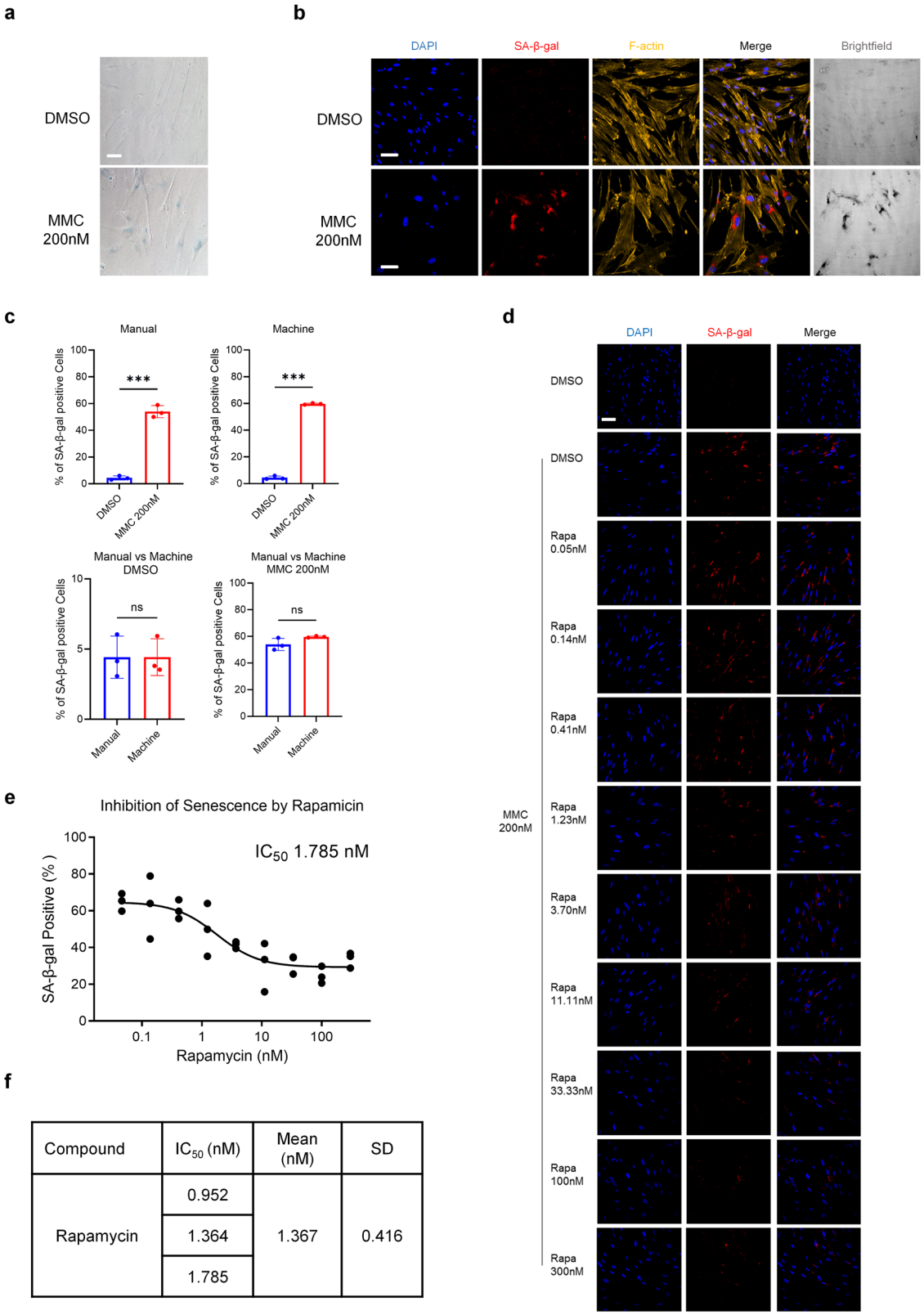

Compound	IC_{50} (nM)	Mean (nM)	SD
Rapamycin	0.952	1.367	0.416
	1.364		
	1.785		

Fig. 1 | Development of a reproducible system for the induction of senescence phenotype and measuring compound potency using fluorescence detection. **a** Representative bright-field images of WI38 cells with SA-β-gal staining after MMC-induced senescence. **b** Fluorescent confocal images of X-gal precipitation with EX640/EM665-705 nm. **c** Analysis of SA-β-gal positive cells in bright-field images manually and in fluorescence images automatically. **d** Representative images of SA-β-gal activity in senescent WI38 cells treated with rapamycin at different concentrations. **e** Dose-response curve of rapamycin on cellular senescence. **f** IC_{50} values for the inhibitory effect of rapamycin on SA-β-gal activity from three independent experiments. All scale bars are 100 μm. *P* values were determined by Unpaired t-test. Data are presented as mean ± SD. ***$P < 0.001$.

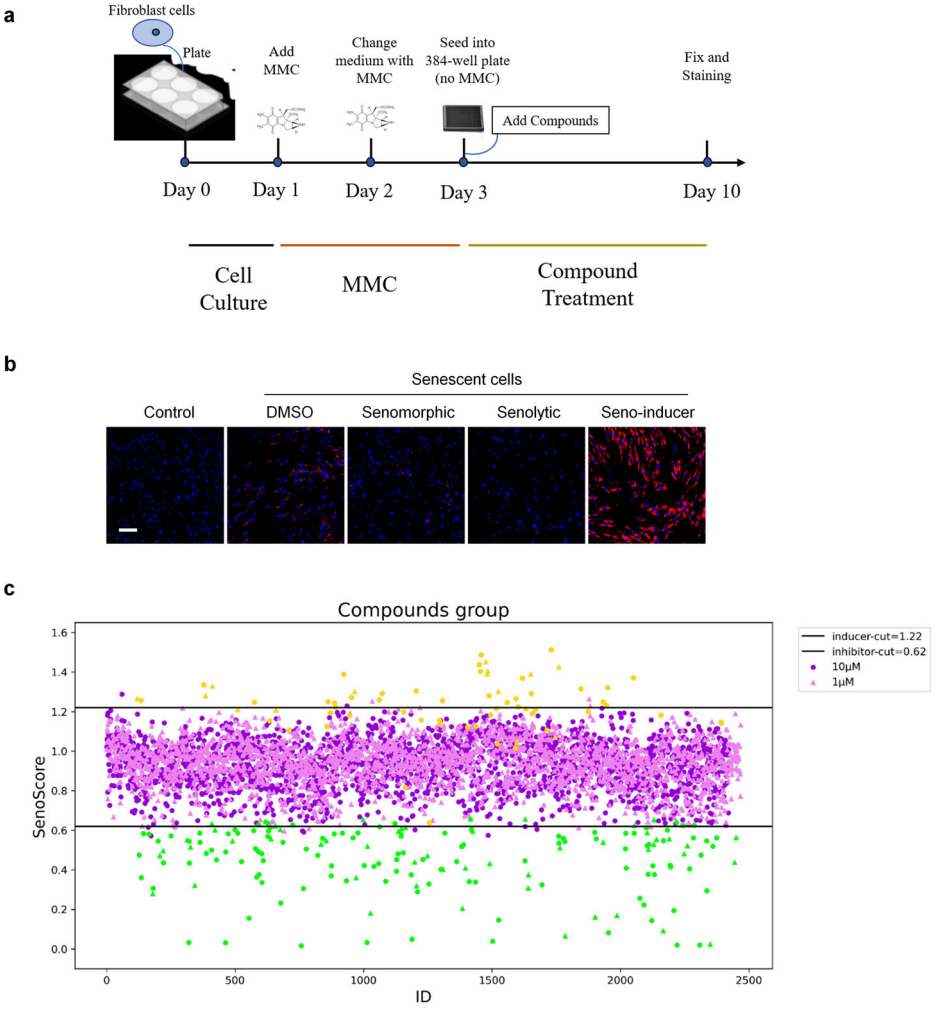

Fig. 2 | Compound screening using the automated fluorescence high throughput screening workflow. a Flowchart of the high-throughput screening experiment workflow for senescence modulators. **b** Representative fluorescent images of SA-β-gal signals after treatment by senomorphic, senolytic and seno-inducer candidates. Control is without MMC treatment while all others have been treated with MMC. **c** Scatter plot showing the SenoScore of 2520 compounds, where the yellow and green data points are positive seno-inducers and inhibitors selected from PositiveRate method for comparison, respectively.

may also be developed to reflect the different nature of senescence heterogeneity[28].

Recent development in machine learning algorithms has been applied to the classification of normal and senescent cells with decent outcomes, either with nuclear features or with label-free bright-field images, with advantages for identifying senescent cells in tissues or patient specimen[15,16,29]. Our method is highly compatible with current fluorescence-based multiplex cellular analysis and is based on direct association with the well-established biomarkers of cellular senescence, without the hassle for complicated training of machine learning models for different cell types, etc. The fluorescent detection of the widely accepted senescence marker SA-β-gal validated here makes it possible for broad applications in new and re-evaluations of historic experimental and pathology specimen in a more quantitative way.

Through technology innovation and integration, optimization and standardization, we have developed an effective and practical experimental and analytic workflow for screening MMC-induced senescence modulators including senomorphic, senolytic, and seno-inducer in a single HCS experiment. For the first time, we introduced a method for the quantitative evaluation of the compound potency on modulating MMC-induced fibroblast senescence. Our system is highly reproducible, accurate, and is a unified system critical for drug development from target identification, high-throughput screen hit discovery, to structure-activity relationship (SAR) studies. We believe this technology innovation could help significantly anti-senescence drug development and senotherapeutic research.

Methods

Cell culture

The human fibroblast cell lines, HDFα (Merck/Sigma-Aldrich, catalog no. 106-05 N), WI-38 (ATCC, catalog no. CCL-75), IMR-90 (ATCC, catalog no. CCL-186) were provided by WuXi AppTec (Shanghai). WI-38 and IMR-90 cells were cultured in EMEM (ATCC, catalog no. 30-2003) and supplemented with 1% Penicillin-Streptomycin solution (HyClone, catalog no. SV30010) and 10% fetal bovine serum (FBS, Excell, catalog no. FSP500). HDFα cells were cultured in FM medium (ScienCell, catalog no. 2301). The cells were kept at 37°C under 5% CO_2 in a water-jacketed cell incubator. For passaging, the adherent cells were trypsinized (0.25%trypsin, Gibco, catalog no. 25200-072), counted using the Vi-CellXR Cell Counter and then re-seeded.

Induction of cellular senescence and compound treatment

Fibroblasts at passage 7, with the cumulative population doublings (CPD) of about 18.1, were seeded into 6-well plate (Corning) at different densities (HDFα 5×10^4/ml, WI-38 and IMR-90 1.5×10^5/ml) and cultured for 24 hours. Then, cells were exposed to low levels of mitomycin C (MMC, Absin, catalog no. 47029279, 200 nM) for 2 × 24 h. After brief rinse, the cells were trypsinized and subcultured into appropriate cell culture vessels without MMC for additional seven days before being fixed and stained for X-gal, and other protein markers.

For compound titration, the MMC-treated cells were seeded into 96- or 384-well plates and treated with blank or compounds or vehicle (0.1% DMSO, Sigma, catalog no. D2650-100ML) controls. For general compound

a

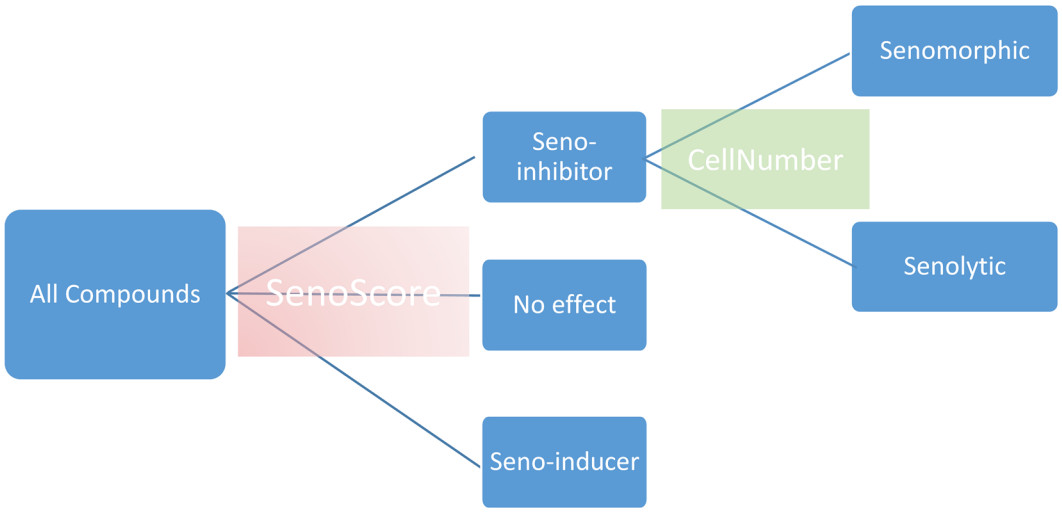

b

Number of Compounds		Positive Compounds				
Total	Excluded*	Category	Total Identified from screen	Reported Positive from Literature	Potential Novel	Missed Reported Positive (From total 2279)
2560	40	Senomorphic	93	29	64	11
		Senolytic	56	12	44	3
		Seno-inducer	34	15	19	23

c

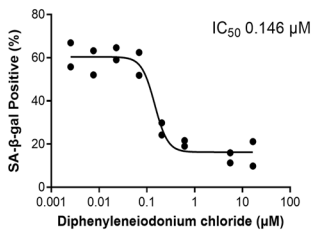

d

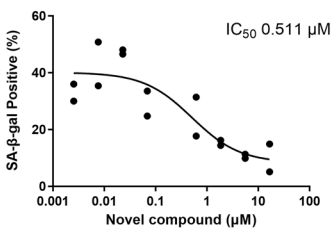

Fig. 3 | Results of compound screening using the automated fluorescence high throughput screening workflow. a Sketch of the compound classification process. **b**, Summary table of the screening results. *Those 40 compounds failing QC criteria in both 1 and 10 μM assays were excluded (Supplementary Fig. 8a step 2). **c** Titration curve of a known senomorphic compound diphenyleneiodonium chloride. **d** Titration curve of a novel senoremedy candidate compound.

screening and titration, Rapamycin (Selleckchem, catalog no. S1039) and KU-60019 (Abcam, catalog no. ab144817) treatment, the cells were treated for 7 days after senescence induction before fixation. During the treatment period, the culture medium was replaced once. For Dasatinib (Beyotime, catalog no. ST023) and Quercetin (Sigma, catalog no. Q4951) (D + Q) treatment, the MMC-induced cells were cultures in medium without MMC for 5 days before being treated with D + Q for 2 days.

SA-β-gal staining and immunofluorescence staining

SA-β-gal activity was assayed using a senescence cell histochemical staining Kit (Sigma, catalog no. CS0030) according to the staining process described previously[4]. Briefly, cells were washed twice with 1X PBS, then added 1X Fixation Buffer and incubated for 6–7 min at room temperature. After 3x rinses, staining mixture was added and cells were incubated at 37°C without CO_2 for 3–4 h, followed with DAPI and Phalloidins (Thermo Fisher Scientific, catalog no. A12380) staining for 1 h. For immunofluorescence staining of $p16^{INK4a}$ (E6N8P Rabbit mAb, Cell Signaling Technology, catalog no. 18769), the cells were fixed with 4% formaldehyde for 15 min. After 3x wash, the cells were blocked for 60 min before being incubated with diluted primary antibody overnight at 4 °C. After 3x rinses, the cells were incubated with secondary antibody (Alexa fluor 488 goat, Invitrogen, catalog no. A11008), DAPI and Phalloidins for 1–2 hours at room temperature in dark. For long-term storage, cells were kept in 1X PBS at 4 °C protected from light.

Compound libraries and the high throughput screening

The compound libraries used in this study were the LOPAC library (1280 compounds, Sigma-Aldrich, catalog no. LO1280) and the Prestwick FDA approved library (1280 compounds) provided by WuXi AppTec (Shanghai). The compound assay plates were prepared with a Labcyte Echo 550 Liquid Handler (Agilent) by transferring 50 nL or 5 nL in duplicates from the source plates into wells of 384-well plates, respectively, while 45 nL DMSO was added into each well of containing 5 nL of compounds. For cell

preparation, the WI-38 cells were seeded into 10 cm^2 dishes at 2×10^6 per dish and cultured 24 h in cell incubator, and then exposed to MMC (200 nM) for 2 × 24 h. Using a Multidrop™ Combi Reagent Dispenser (Thermo Scientific, USA), 5000 MMC-induced cells were seeded in 50 µl per well into 384-well plates, with the final compound concentrations at 1 µM or 10 µM. After 7 days, the cells were fixed and stained as described above. Rapamycin was used as a positive compound in the screen while DMSO (0.1% final) was used as vehicle control. To exclude the edge effect, the wells in the most outer rows or columns close to the edge of a 384-well plate were not used for cell culture. Instead, these wells were filled with culture medium. The compound screening was done in 40 384-well plates with average Z' factor at 0.435.

Image acquisition and analysis

The bright-field images of Fig. 1a were captured with an inverted microscope (Nikon, Japan) at 20× objective. Five distinct fields of view per well were acquired for manual identification of positive cells.

For compound titration and screen, bright-field and fluorescence images were captured using a high-content analysis system (CQ1 Confocal Quantitative Image Cytometer, Yokogawa, Japan). The images stacks were collected from one bright-field and four fluorescence channels with a 20X objective. For compound titration assays, images were acquired from 20 distinct fields of view per well using a 96-well plate. For high-throughput compound library screening, 384-well plates were used, with 4 fields captured per well. All acquired fields of view were included in the subsequent analyses for both titration and screening experiments. Unless otherwise mentioned, the images were captured sequentially according to the following. Channel 1 was for nuclear DAPI (Ex405nm, Em447/60 nm), 400 ms exposure; Channel 2 for SA-β-gal (Ex640 nm, Em685/40nm), 300 ms exposure; Channel 3 for F-actin (Ex561nm, Em585/29 nm), 500 ms exposure; Channel 4 for $p16^{INK4a}$ protein (Ex488nm, Em525/50 nm), 370 ms exposure; and Channel 5 for SA-β-gal in bright-field, 50 ms exposure.

For comparison, an Operetta® CLS High Content Imaging System (PerkinElmer, USA) equipped with a Bright-field Module, LED light sources, Operetta Software and a 20X objective was used to capture cell images from 25 fields per well of a 96-well plate with the same fluorescence settings.

For image analysis, software came with the CQ1 (CQ1 Measurement and analysis software) or Operetta system (Harmony High-Content Imaging and Analysis Software) were used. The nuclear DAPI channel was used for nuclei and cell identification and counting, as well as the calculation of nuclear area[14]. The F-actin staining (Alexa Fluor 568 Phalloidin) was used for the identification of the cell cytoplasmic boundary and cell segmentation. The X-gal precipitate signal within each cell boundary was used for SA-β-gal activity measurement and positive cell counting. The quantification and analysis of $p16^{INK4a}$ fluorescence intensity of each cell were carried the same way.

Workflow for data processing and analysis

The equations for calculation and workflow were illustrated in Supplementary Fig. 8. The brief description is the following:

1. Identification of SA-β-gal positive cells. The mean intensity of X-gal signal of each cell ($Cell_{SA-\beta-gal}$) was calculated from the CQ1 software. For each plate, the cutoff value l of SA-β-gal positive cells was calculated according equation (1) (Supplementary Fig. 8a,b) for identifying SA-β-gal positive cells, where the number 0.75 (3/4) is determined empirically. The $p16^{INK4a}$ positive cells were counted similarly to the SA-β-gal positive cells.
2. The NucleusArea of each well was the median of all cells in each well from the CQ1 software.
3. The SA-β-gal positive rate of each well was calculated according equation (3) (Supplementary Fig. 8a,b).
4. For exclusion of abnormal wells in the HTS screening, two criteria were used. (a) the difference between the duplicates in PositiveRate is larger than 2-fold; or (b) the cell count in each well is smaller than γ (equation (4), Supplementary Fig. 8a), where the number 0.6 is common criteria used in cell viability assay for compound toxicity for excluding highly toxic compounds.
5. For compound screening. We introduced SenoScore calculated according equation (1) (Supplementary Fig. 8c), which weighed in both the PositiveRate and NucleusArea.

It should be noted that an empirical value of 0.75 (3/4) was used as coefficient in Equation (1) in our calculation of the λ value for identifying SA-b-gal positive cells. This coefficient, typically ranges from 0 to 1 depending on the senescence-inducing and experimental conditions, should be optimized at the start of the project based on the manual counting and validation results from rigorously designed preliminary experiments with both positive and negative controls. Both positive and negative controls should be included in every assay plate as well.

Metadata analysis of compound classification

The classification of reported senomodifiers in Fig. 2e and Supplementary Fig. 9b, c were done with PubMed search, artificial intelligence (AI) assisted search (Bohrium, Perlexity, and Co-Pilote), compound structure analysis, and human expert curation. Briefly, the common names of all compounds were searched in PubMed together with cellular senescence, SA-beta-gal, beta-galactosidase, and SASP through all available timeframe. Then, batches of compound names were asked in the AI-assisted search engine if they are senomorphic, senolytic, or senoinducer. Human experts examined all the results, together with compound structures if needed, and made the final decision.

qRT-PCR

Total RNA was extracted from cells using RNeasy Plus Mini Kit from Qiagen. cDNA synthesis was performed using High Capacity cDNA Reverse Transcription Kit from Applied Biosystems. qPCR reactions were performed with PowerUp™ SYBR™ Green Master Mix from Applied Biosystems. Thermal cycling conditions consisted of an initial hold at 50 °C for 2 min followed by a hold at 95 °C for 10 min. This was followed by a two-step PCR program consisting of 40 cycles of 95 °C for 15 s and 60 °C for 60 s. Primer sequences are listed in Supplementary Table 2.

ELISA

The cells were induced and treated as described above for total of 10 days. At the end of the 10 days, the cells in 96-well plates were rinsed and cultured in serum-free EMEM medium for 24 hours before the medium were collected for ELISA analysis of cytokines. The Human IL-6 Quantikine ELISA Kit (R&D systems, catalog no. D6050) was used for the quantification of IL-6 in the cell culture medium following the procedures described by the manufacturer.

Western Blot

Protein from WI-38 cells were lysed in RIPA buffer (Sigma, catalog no. R0278) with Protease & Phosphatase Inhibitor (Thermo Fisher Scientific, catalog no. 78440). All protein lysates were quantified using Pierce™ BCA Protein Assay Kits (Thermo Fisher Scientific, catalog no. 23225). A total of 10–50 µg of total protein was loaded and separated on 4–12% Bis-Tris gels (Invitrogen, catalog no. NP0336BOX), and dry transferred to nitrocellulose membrane (Invitrogen, catalog no. IB23001). The membranes were blocked for 1 h with blocking buffer and incubated with primary antibodies overnight at 4 °C, washed 3 times with 1X TBST (Invitrogen, catalog no. 28360) and incubated 1 h with secondary antibodies at room temperature.

Finally, membranes were washed 3 times with 1X TBST and protein expression levels were quantified using chemiluminescent reagents (Thermo Fisher Scientific, catalog no. 34096). Antibodies used in the study were rabbit anti-$p16^{INK4a}$ Rabbit mAb antibody (1:1000, Cell Signaling Technology, catalog no. 80772S), mouse anti-p21 antibody (1:300, p21/CIP1/WAF1/CDKN1A Antibody, Novus Biologicals, catalog no. NBP2-29463-20ug), rabbit anti-GAPDH antibody (1:10000, GAPDH Rabbit

mAb, Cell Signaling Technology, catalog no. 2118S). The secondary antibodies, anti-mouse and anti-rabbit IgG (1:10000), were obtained from Proteintech®.

Statistics and Reproducibility

Data are presented as mean ± SD, and the number of biological replicates (n) for each experiment was specified. Differences in means were analyzed using one-way ANOVA, and unpaired two-tailed Student's t test for two groups. Unless otherwise indicated, the data were obtained from three independently performed biological replicates. A probability value of p smaller than 0.05 was considered statistically significant (*, $p \le 0.05$; **, $p \le 0.01$; ***, $p \le 0.001$; and ****, $p \le 0.0001$). GraphPad Prism 9.0 software was used for statistical analysis and plotting.

Reporting summary

Further information on research design is available in the Nature Portfolio Reporting Summary linked to this article.

Data availability

The data that support the findings of this study are available from the corresponding author upon reasonable request. The source data for the graph has been provided as Supplementary Data 1. Uncropped blots supporting the findings of this study are provided in the Supplementary Information.

Received: 9 January 2025; Accepted: 21 August 2025;
Published online: 30 August 2025

References

1. Rhinn, M., Ritschka, B. & Keyes, W. M. Cellular senescence in development, regeneration and disease. *Development* **146**, dev151837 (2019).
2. Kirkland, J. L. & Tchkonia, T. Cellular senescence: a translational perspective. *EBioMedicine* **21**, 21–28 (2017).
3. Di Micco, R., Krizhanovsky, V., Baker, D. & d'Adda di Fagagna, F. Cellular senescence in ageing: from mechanisms to therapeutic opportunities. *Nat. Rev. Mol. Cell Biol.* **22**, 75–95 (2021).
4. Dimri, G. P. et al. A biomarker that identifies senescent human cells in culture and in aging skin in vivo. *Proc. Natl. Acad. Sci. USA* **92**, 9363–9367 (1995).
5. Lundberg, A. S., Hahn, W. C., Gupta, P. & Weinberg, R. A. Genes involved in senescence and immortalization. *Curr. Opin. Cell Biol.* **12**, 705–709 (2000).
6. Baker, D. J. et al. Clearance of p16 Ink4a-positive senescent cells delays ageing-associated disorders. *Nature* **479**, 232–236 (2011).
7. Gorgoulis, V. et al. Cellular senescence: defining a path forward. *Cell* **179**, 813–827 (2019).
8. Suryadevara, V. et al. SenNet recommendations for detecting senescent cells in different tissues. *Nat. Rev. Mol. Cell Biol.* https://doi.org/10.1038/s41580-024-00738-8 (2024).
9. Bitler, B. G., Fink, L. S., Wei, Z., Peterson, J. R. & Zhang, R. A high-content screening assay for small-molecule modulators of oncogene-induced senescence. *J. Biomol. Screen.* **18**, 1054–1061 (2013).
10. Fuhrmann-Stroissnigg, H. et al. Sa-β-galactosidase-based screening assay for the identification of senotherapeutic drugs. *J. Vis. Exp.* **2019**, 1–7 (2019).
11. Li, X. et al. First-generation species-selective chemical probes for fluorescence imaging of human senescence-associated β-galactosidase. *Chem. Sci.* **11**, 7292–7301 (2020).
12. Ogawa, S. et al. Rapid fluorescence imaging of human hepatocellular carcinoma using the β-galactosidase-activatable fluorescence probe SPiDER-β. *Gal. Sci. Rep.* **11**, 1–12 (2021).
13. Biran, A. et al. Quantitative identification of senescent cells in aging and disease. *Aging Cell* **16**, 661–671 (2017).
14. Chan, K. T. et al. Combining high-content imaging and phenotypic classification analysis of senescence-associated beta-galactosidase staining to identify regulators of oncogene-induced senescence. *Assay. Drug Dev. Technol.* **14**, 416–428 (2016).
15. Kusumoto, D. et al. Anti-senescent drug screening by deep learning-based morphology senescence scoring. *Nat. Commun*. **12**, 257 (2021).
16. Duran, I. et al. Detection of senescence using machine learning algorithms based on nuclear features. *Nat. Commun*. **15**, 1041 (2024).
17. Matei, V. A. et al. Near-infrared laser illumination transforms the fluorescence absorbing X-Gal reaction product BCI into a transparent, yet brightly fluorescent substance. *Brain Res. Bull.* **70**, 33–43 (2006).
18. Levitsky, K. L., Toledo-Aral, J. J., López-Barneo, J. & Villadiego, J. Direct confocal acquisition of fluorescence from X-gal staining on thick tissue sections. *Sci. Rep.* **3**, 1–6 (2013).
19. Campisi, J. Cellular senescence: putting the paradoxes in perspective. *Curr. Opin. Genet. Dev.* **21**, 107–112 (2011).
20. Alili, L., Diekmann, J., Giesen, M., Holtkötter, O. & Brenneisen, P. A drug-induced accelerated senescence (DIAS) is a possibility to study aging in time lapse. *Age* **36**, 1329–1343 (2014).
21. Selvarani, R., Mohammed, S. & Richardson, A. Effect of rapamycin on aging and age-related diseases—past and future. *GeroScience* **43**, 1135–1158 (2021).
22. Coppé, J.-P., Desprez, P.-Y., Krtolica, A. & Campisi, J. The senescence-associated secretory phenotype: the dark side of tumor suppression. *Annu. Rev. Pathol. Mech. Dis.* **5**, 99–118 (2010).
23. González-Gualda, E., Baker, A. G., Fruk, L. & Muñoz-Espín, D. A guide to assessing cellular senescence in vitro and in vivo. *FEBS J.* **288**, 56–80 (2021).
24. Park, J. H. et al. Pharmacological inhibition of mTOR attenuates replicative cell senescence and improves cellular function via regulating the STAT3-PIM1 axis in human cardiac progenitor cells. *Exp. Mol. Med.* **52**, 615–628 (2020).
25. Kang, H. T. et al. Chemical screening identifies ATM as a target for alleviating senescence. *Nat. Chem. Biol.* **13**, 616–623 (2017).
26. Lagoumtzi, S. M. & Chondrogianni, N. Senolytics and senomorphics: Natural and synthetic therapeutics in the treatment of aging and chronic diseases. *Free Radic. Biol. Med.* **171**, 169–190 (2021).
27. Shaito, A. et al. Potential adverse effects of resveratrol: a literature review. *Int. J. Mol. Sci*. **21**, 2084 (2020).
28. Tao, W., Yu, Z. & Han, J.-D. J. Single-cell senescence identification reveals senescence heterogeneity, trajectory, and modulators. *Cell Metab.* **36**, 1126–1143.e5 (2024).
29. Heckenbach, I. et al. Nuclear morphology is a deep learning biomarker of cellular senescence. *Nat. Aging* **2**, 742–755 (2022).

Acknowledgements

We would like to thank Ms. Yan Hu, Mr. YanJun Mao and Hong Zou at Sequanta Technologies Co., Ltd. (Shanghai) for providing cytokine analysis using OLink® Inflammation panel. We would like to thank the DP Technology (https://bohrium.dp.tech/) support team, Dr. Dachao Cui, and Mr. Haibin Wang for their diligent work on assisting the confirmation of the known small molecule senescence modulators. We would also like to thank Drs. Henry Lu and Letian Kuai for their continuous support throughout this project and helpful discussions.

Author contributions

T.L. conceived the study; T.L., T.H., and TH.Z. provided supervision; YJ.H., TH.Z., T.H., and T.L. designed experiments and wrote the protocols; YJ.H., TH.Z. and Y.L. did the experiments; XQ.X., YJ.H., T.H., Y.L., PC Z. and T.L. analyzed data; All authors participated in discussion. YJ.H., T.H. and T.L wrote the original draft; and T.L. wrote the final manuscript.

Competing interests

The project was supported by internal grants to T.L. from WuXi AppTec. The method was submitted for patent application. The authors declare no competing interests.

Additional information

Supplementary information The online version contains supplementary material available at https://doi.org/10.1038/s42003-025-08758-6.

Correspondence and requests for materials should be addressed to Tao Lu or Peichuan Zhang.

Peer review information *Communications Biology* thanks Laura R. Sinclair and the other, anonymous, reviewer(s) for their contribution to the peer review of this work. Primary Handling Editor: Ophelia Bu. A peer review file is available.